Configuration mixing of angular momentum projected self-consistent mean-field states for neutron-deficient Pb isotopes

M. Bender,[1] P. Bonche,[2] T. Duguet,[3] and P.-H. Heenen[1]
[1]*Service de Physique Nucléaire Théorique, Université Libre de Bruxelles, Case Postale 229, B-1050 Bruxelles, Belgium*
[2]*Service de Physique Théorique, CEA Saclay, 91191 Gif sur Yvette Cedex, France*
[3]*Physics Division, Argonne National Laboratory, Argonne, Illinois 60439, USA*
(Received 24 November 2003; published 2 June 2004)

We study the low-lying collective excitation spectra of the neutron-deficient lead isotopes $^{182-194}$Pb by performing a configuration mixing of angular momentum and particle-number projected self-consistent mean-field states. The same effective interaction is used to generate the mean-field states and for the configuration mixing. We choose the Skyrme interaction SLy6 supplemented by a density-dependent zero-range pairing force. Our study supports the interpretation of the excitation spectra made on the grounds of more schematic models in terms of coexisting spherical, oblate, prolate, and superdeformed prolate structures. The model qualitatively reproduces the variation of the spectra with neutron number. Our results for $E0$ and $E2$ transition probabilities are compared with the few existing experimental data. Finally, we predict the presence of superdeformed bands at low excitation energy in the most neutron-deficient isotopes.

DOI: 10.1103/PhysRevC.69.064303 PACS number(s): 21.60.Jz, 21.10.Pc, 27.70.+q, 27.80.+w

I. INTRODUCTION

The neutron-deficient lead isotopes have been the subject of intense experimental studies for nearly 20 years [1]. This continuous interest is mainly motivated by their rich excitation spectra which strongly depend on the neutron number. First evidence for low-lying 0^+ states in $^{182-194}$Pb was obtained from β^+-decay and electron capture of adjacent Bi isotopes [2,3]. At least one low-lying excited 0^+ state has now been observed in all even-even Pb isotopes between ^{182}Pb and ^{194}Pb at excitation energies below 1 MeV. In particular, ^{186}Pb [4] is a unique example of a fermion system where the two lowest excited states are 0^+ levels with energies below 700 keV. For this nucleus it has also been shown that the yrast band is based on states with a sizable prolate deformation [5–7].

The $Z=82$ proton shell closure has been shown to be stable up to very neutron-deficient Pb isotopes [8]. The excited 0^+ states have been interpreted within two different frameworks, the mean field and the shell models. The apparently different mechanisms leading to these states within the two approaches have been shown to be complementary views of the same phenomenon [9]. Both models can explain the experimental data qualitatively.

In a mean-field approach, the spectra of the Pb isotopes are understood as reflecting several competing minima in an axial quadrupole energy landscape, corresponding to spherical, oblate, and prolate deformations. The very name "shape coexistence phenomenon" comes from this mean-field description [9,10]. It is present in most nuclei around the Pb isotopes [1] and has been found also in other regions of the mass table [9]. First calculations based on phenomenological mean fields have predicted the existence of several competing minima in the deformation energy surface of neutron-deficient Pb isotopes [11–13] and a transition from oblate to prolate isomers [14]. More recently, several variants of the self-consistent mean-field approach have confirmed these results [15–18]. However, in the neutron-deficient Pb region, shape coexistence cannot be completely described at the level of mean-field models. The minima obtained as a function of the quadrupole moment are often rather shallow and it is not clear *a priori* whether they will survive dynamical effects such as quadrupole vibrations.

In a shell-model picture, the excited 0^+ states are generated by np-nh proton excitations across the $Z=82$ shell gap, from the $3s_{1/2}$ level to the $1h_{9/2}$. The excitation energies are lowered by a residual quadrupole-quadrupole interaction. From this point of view, the mean-field oblate minimum is associated with a proton $2p$-$2h$ configuration and the prolate one with proton $4p$-$4h$ intruder states [19]. Many-particle–many-hole excitations cannot be easily handled in full-scale shell-model calculations, in particular, for the large model space required for the description of heavy open-shell nuclei. They are, therefore, treated with the help of algebraic models [20,21].

A third, purely phenomenological, approach has also been used to interpret the experimental findings: the shape-mixing picture [9]. In this model, the physically observed states are the result of the interaction between several configurations. They are thus a superposition of spherical, oblate, and prolate configurations, the relative weights in the mixing being determined by a fit to the experimental data. Systematic two-level mixing calculations for $^{190-200}$Pb have been presented in Ref. [22]. A simple two-level mixing model has been applied to the analysis of the α-decay hindrance factors in Ref. [23]. Three level mixing has been performed in Refs. [24,25] for ^{188}Pb. Let us also recall that, in such models, the strength of monopole transitions is related to the value of the interaction matrix elements between the unperturbed configurations [26].

The aim of this paper is to provide a unified view of mean-field and shape mixing approaches. The method that we use has been presented in Ref. [27] and applied to the study of shape coexistence in ^{16}O in Ref. [28]. Results for

^{186}Pb have already been published in Ref. [29]. As a starting point, the method uses self-consistent mean-field wave functions generated as a function of the axial quadrupole moment. Particle number and angular momentum are restored by projecting these wave functions on the correct numbers of neutrons and protons and on spin. Finally, a mixing of the projected wave functions corresponding to different quadrupole moments is performed with a discretized version of the generator coordinate method. One of the appealing features of our method is that its only phenomenological ingredient is the effective nucleon-nucleon interaction which has been adjusted once and for all on generic nuclear properties. Another attractive aspect is the direct determination of electric transition probabilities between any pair of states in the laboratory frame.

There have already been studies of the Pb isotopes along similar lines. Tajima *et al.* [15] and Chasman *et al.* [17] have used a very similar framework, but without any symmetry restoration. Mixing of microscopic self-consistent mean-field wave functions has been approximated by Libert *et al.* [16] using a macroscopic Bohr Hamiltonian. Let us also mention that Fossion *et al.* [21] have performed three-configuration mixing calculations within the IBM formalism.

II. FRAMEWORK

The starting point of our method is a set of HF+BCS wave functions $|q\rangle$ generated by self-consistent mean-field calculations with a constraint on a collective coordinate q. In the language of the nuclear shell model, such mean-field states incorporate particle-particle (pairing) correlations as well as many-particle–many-hole correlations by allowing for the deformation of the nucleus in the intrinsic frame. As a consequence, however, such mean-field states break several symmetries of the exact many-body states. The symmetry violation causes some difficulties, for instance, when relating the mean-field results to spectroscopic data obtained in the laboratory frame. Eigenstates of the angular momentum and the particle number operators are obtained by restoration of rotational and particle-number symmetry on each intrinsic wave function $|q\rangle$:

$$|JMq\rangle = \frac{1}{\mathcal{N}_{JMq}} \sum_K g_K^J \hat{P}_{MK}^J \hat{P}_Z \hat{P}_N |q\rangle, \tag{1}$$

where $\mathcal{N}_{JMq}$ is a normalization factor; $\hat{P}_{MK}^J$, $\hat{P}_N$, $\hat{P}_Z$ are projectors onto the angular momentum J with projection M along the laboratory z axis and K in the intrinsic z axis, neutron number N and proton number Z, respectively. Here, we impose axial symmetry and time-reversal invariance on the intrinsic states $|q\rangle$. Therefore, K can only be 0 and one can omit the coefficients $g_K^J = \delta_{K0}$ as well as the sum over K. A variational configuration mixing on the collective variable q is performed for each J value separately,

$$|JMk\rangle = \sum_q f_{J,k}(q) |JMq\rangle. \tag{2}$$

The weight functions $f_{J,k}(q)$ are determined by requiring that the expectation value of the energy

$$E_{J,k} = \frac{\langle JMk|\hat{H}|JMk\rangle}{\langle JMk|JMk\rangle} \tag{3}$$

is stationary with respect to an arbitrary variation $\delta f_{J,k}^*(q)$. This prescription leads to the discretized Hill-Wheeler equation [30]. Collective wave functions in the basis of the intrinsic states are then obtained from the set of weight functions $f_{J,k}(q)$ by a basis transformation [15]. In the $|JMk\rangle$ wave functions, the weight of each mean-field state $|q\rangle$ is given by

$$g_{J,k}(q) = \langle JMk|JMq\rangle. \tag{4}$$

Since the collective states $|JMk\rangle$ have good angular momentum, their quadrupole moments and transition probabilities can be determined directly in the laboratory frame without further approximation. As the full model space of occupied single-particle states is used, no effective charge needs to be introduced. The formulas used to evaluate the overlap and Hamiltonian matrix elements have been presented in Ref. [27].

The same effective interaction is used to generate the mean-field wave functions and to carry out the configuration mixing calculations. We have chosen the Skyrme interaction SLy6 in the mean-field channel [31] and a density-dependent zero-range pairing force with a strength of -1250 MeV fm^3 for neutrons and protons in connection with a soft cutoff at 5 MeV above and below the Fermi energy as defined in Ref. [32]. A model that combines these extensions of the mean-field approach represents a powerful tool. From a numerical point of view, it is still simple enough to be applied up to superheavy nuclei using the full model space of single-particle states with the proper coupling to the continuum. Correlations corresponding to collective modes can be incorporated step by step into the modeling and this helps to identify the relevant degrees of freedom. The method has the advantage that results can be interpreted within the intuitive picture of intrinsic shapes and shells of single-particle states that is usually offered by mean-field models.

The model has already been successfully applied to the description of coexisting structures in ^{16}O [28] and ^{32}S, ^{36,8}Ar, and ^{40}Ca [33]. Results for ^{186}Pb obtained with this model have already been presented in Ref. [29].

III. RESULTS

A. Potential landscapes

The potential energy and other properties are plotted as a function of a dimensionless quadrupole deformation parameter approximately independent of the nuclear mass

$$\beta_2 = \sqrt{\frac{5}{16\pi}} \frac{4\pi\sqrt{Q_{20}^2 + 2Q_{22}^2}}{3R^2A}, \tag{5}$$

where $Q_{2\mu}$ is the expectation value of the operator

$$Q_{\lambda,\mu} = r^\lambda Y_{\lambda,\mu} \tag{6}$$

for $\lambda = 2$.

The particle-number projected potential energy curves are displayed in Fig. 1. For all neutron numbers, the ground state

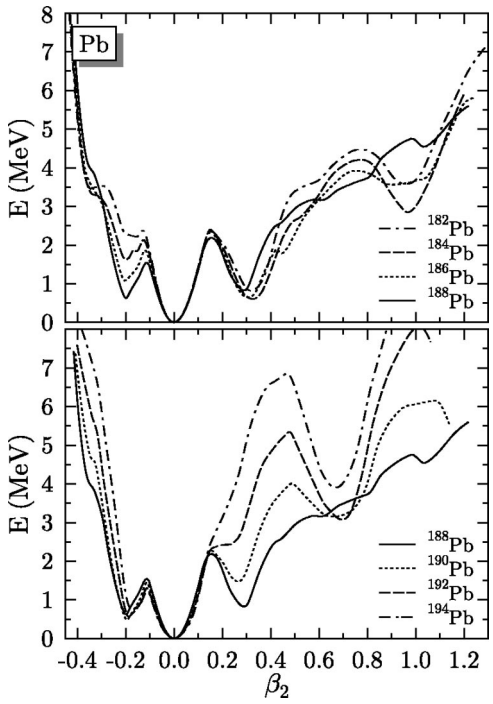

FIG. 1. Particle-number projected deformation energy curves for $^{182-188}$Pb (upper panel) and $^{182-194}$Pb (lower panel). The curve for ^{188}Pb is shown in both panels.

is found to be spherical with a similar curvature of the energy curve around the spherical point. There is a well defined, slightly deformed, oblate minimum for all isotopes. Its excitation energy increases while the depth of the well decreases when going down in neutron number from ^{188}Pb to ^{182}Pb. On the prolate side, an inflexion point in the $^{192-194}$Pb curves becomes a well-deformed minimum for β_2 varying from 0.30 for ^{190}Pb to 0.35 for ^{182}Pb. The deformation energy curves also present a deep minimum at superdeformed shapes for $^{194-192}$Pb which becomes shallower in ^{190}Pb, and disappears for the lighter isotopes. For the three lightest isotopes, there is an additional minimum at still larger deformations, with a maximal depth of 1.5 MeV for ^{184}Pb.

Exploratory studies performed by Ćwiok [34] indicate that calculations performed with a zero-range volume pairing interaction with appropriate strengths result in oblate and prolate minima at energies close to the experimental values. However, since our aim is to determine the influence of correlations beyond mean field for interactions that have been validated on a large set of data, we will limit ourselves to the same form of pairing as used in previous works.

For deformations between $\beta_2=-0.3$ and $\beta_2=+0.4$, the variation of energy does not exceed 2.5 MeV in $^{182-190}$Pb. The barrier heights between the minima are slightly larger than 2 MeV for the prolate and some superdeformed minima. In contrast, the barrier heights between spherical and oblate minima are always small. With such a topology, most minima of the potential energy curves cannot be unambiguously identified with physical states and one can speculate whether these structures may be washed out by the vibrational fluctuations associated with quadrupole motion. As discussed on the basis of phenomenological energy maps for neutron-deficient Pb isotopes by Bengtsson and Nazarewicz [12], it is hard to infer the effect of vibrational fluctuations only from the topology of the potential landscape.

In principle, oblate and prolate minima found by a calculation limited to axial deformation might be connected by a path through triaxial quadrupole deformation. To verify that this is not the case for the Pb isotopes, we have calculated the two-dimensional energy maps for four isotopes. They are displayed in Fig. 2. The triaxial deformation angle γ is defined by

$$\tan(\gamma) = \sqrt{2}\frac{Q_{22}}{Q_{20}}. \tag{7}$$

The potential maps for ^{182}Pb and ^{194}Pb exhibit two minima at small deformations, spherical and oblate for ^{194}Pb and spherical and prolate for ^{182}Pb, while three stable minima can be seen for the two other isotopes. The barrier height between the prolate and oblate minima is larger than 500 keV. In ^{190}Pb, the prolate minimum is slightly triaxial with $\gamma \approx 10°$.

The energy curves obtained after projection on angular momentum $J=0$ are shown in Fig. 3. As can be seen, the conclusions drawn from Fig. 1 remain qualitatively valid. The spherical mean-field state is rotationally invariant and, therefore, contributes to $J=0$ only. As found in previous studies of spherical nuclei with our method, there are two minima at small deformations. They do not represent distinct physical states, but, as will be clear after the configuration-mixing calculation, the correlated spherical state. The depth of the oblate well is affected by angular momentum projection, as the barrier separating it from the spherical minimum is quite low for all neutron numbers.

B. Single-particle spectrum

The minima obtained for specific deformations are associated with a shell effect due to a low level density around the Fermi energies for both protons and neutrons. To visualize this effect, we show Nilsson plots of the proton and neutron single-particle energies for ^{186}Pb in Figs. 4 and 5, respectively. Besides an overall offset due to the change in proton-neutron asymmetry, the proton spectra are similar for other neutron numbers. These curves are also quite close to those presented in Ref. [15], where a different set of Skyrme and pairing parameters was used.

The spherical gap ($\beta_2=0$) dominates the proton spectrum, There is also a spherical neutron subshell closure at $N=100$ between the $2f_{7/2^-}$ and $1i_{13/2^+}$ levels. Several additional, smaller gaps are visible at various deformations; let us first focus on the oblate side.

A large proton shell gap is present for an oblate deformation $\beta_2 \approx -0.2$. Comparing the level ordering at this deformation with that at sphericity indicates that the $3s_{1/2^+}$ levels have been pushed up from below the Fermi energy and have crossed two down-sloping $1h_{9/2^-}$ levels. The deformation at which the first level crossing occurs depends predominantly on the size of the spherical $Z=82$ gap: the larger the gap, the larger the deformation of the oblate minimum, as this crossing corresponds to the position of the barrier between the

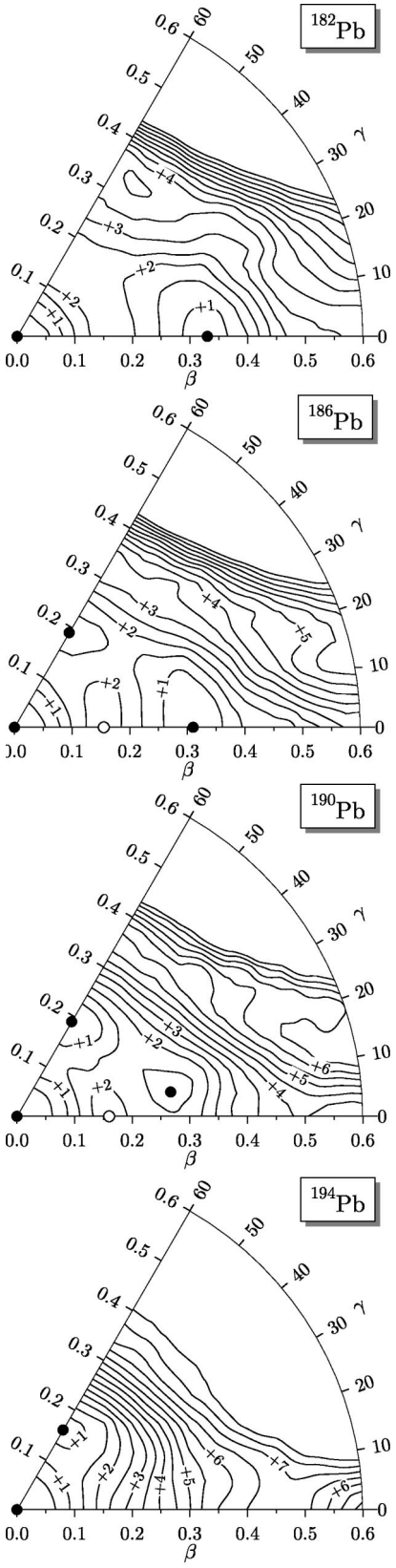

FIG. 2. Particle-number projected deformation energy surfaces for the Pb isotopes as indicated. The contour lines are separated by 0.5 MeV. Filled circles denote minima, open circles maxima of the potential landscape.

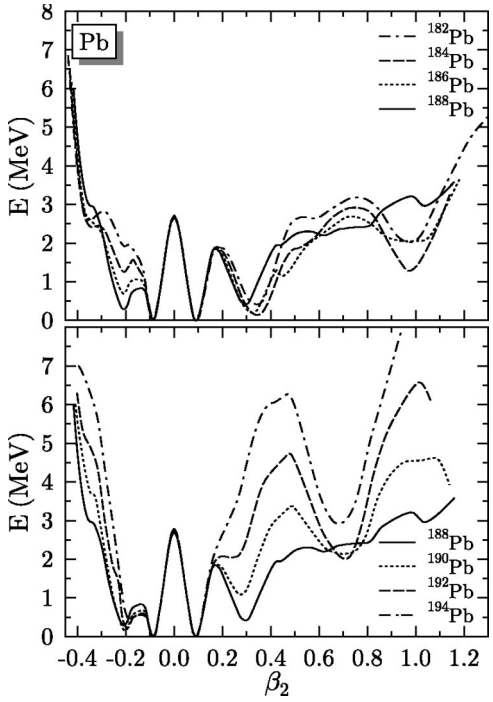

FIG. 3. Particle-number and angular momentum $J=0$ projected deformation energy curves for $^{182-194}$Pb drawn in the same manner as in Fig. 1. All curves are normalized to the energy minimum.

oblate and the spherical energy minima. In a shell-model picture [19,20], this oblate state is described by a $2p$-$2h$ excitation from the $3s_{1/2^+}$ level to the $1h_{9/2^-}$ one.

The size of the oblate proton gap is mainly determined by the splitting of the $1h_{9/2^-}$ state with deformation, which can be expected to be force independent. It depends also on the energy difference between the $1h_{9/2^-}$ and the $1i_{13/2^+}$ levels, which has to be large enough so that the $1i_{13/2^+}$ states diving down with oblate deformation stay above the oblate $2p$-$2h$ gap. That the level closest to the Fermi level is a $1h_{9/2^-}$ state is supported by the fact that in adjacent even-odd Tl and Bi nuclei, states built on the proton $1h_{9/2^-}$ orbital above and the $3s_{1/2^+}$ orbital below the $Z=82$ gap have been observed at excitation energies of only a few hundred keV [35].

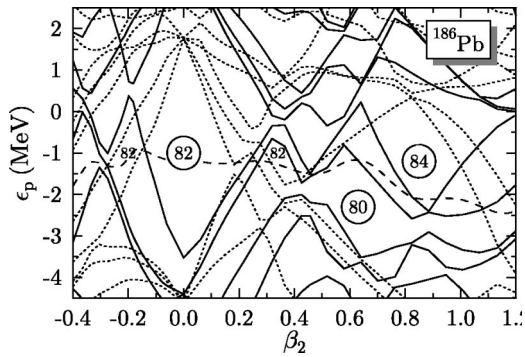

FIG. 4. Proton eigenvalues of the single-particle Hamiltonian for ^{186}Pb. Solid lines denote states with positive parity, dotted lines states with negative parity. The Fermi energy is plotted with a dashed line.

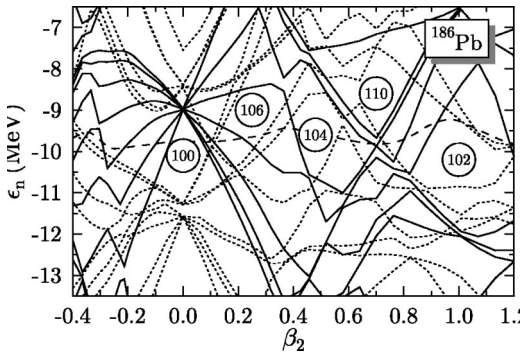

FIG. 5. Eigenvalues of the single-particle Hamiltonian obtained for neutrons in ^{186}Pb. Solid lines denote states with positive parity, dotted lines states with negative parity. The Fermi energy is plotted with a dashed line.

This interpretation of the oblate states is also consistent with the observation of 11^- high-spin isomers for $^{188-198}$Pb [1]. These isomers are interpreted as broken-pair proton $(3s_{1/2}^{-2}1h_{9/2}1i_{13/2})_{11^-}$ states. The values of their g factor and of their spectroscopic quadrupole moment have been measured in $^{194-196}$Pb [36] and are consistent with excitations built on top of the excited 0^+ oblate states. They have been successfully described in this way by Smirnova *et al.* [37].

The level ordering shown in Fig. 4 is thus corroborated by several experimental data and gives a coherent picture of the oblate minimum. The situation is less evident for the neutrons. As can be seen from Fig. 5, the levels which are responsible for the oblate neutron gap originate from the $1h_{9/2^-}$ and $1i_{13/2^+}$ shells. Their first crossings occur at deformations around $\beta_2 \approx -0.2$; only two $1i_{13/2^+}$ levels have energies lower than the Fermi energy at the oblate minimum of ^{186}Pb.

As we shall show in the next sections, the energy of the predominantly oblate 0^+ state is overestimated for all isotopes by our model. A possible cure to this deficiency could thus be to slightly decrease the energy of the $1i_{13/2^+}$ neutron level. A larger occupation of these neutron states with large m_z values would increase the quadrupole interaction between neutrons and protons, the proton levels close to the Fermi energy having also large m_z values. This would decrease the energy of the oblate configuration and modify its dependence on the neutron number. There are other evidences that the $1i_{13/2^+}$ energy is overestimated. On the prolate side of deformations, levels from the spherical proton $1i_{13/2^+}$ and $1h_{9/2^-}$ shells come close to the Fermi energy in the ground state of transactinides. An analysis of the quasiparticle spectrum of ^{249}Bk performed in the cranked Hartree-Fock-Bogoliubov approach using the Skyrme interaction SLy4 in combination with the same pairing prescription used here indicates that the $1i_{13/2^+}$ state is predicted too high above the $1h_{9/2^-}$ orbital and should be lowered [38]. A similar conclusion emerges from the analysis of the single-particle spectra in ^{208}Pb, where most mean-field models predict the proton $1i_{13/2^+}$ shell too far above the $1h_{9/2^-}$ level [39,40]. As we discussed above, however, these single-particle energies are also constrained by the properties of oblate states around ^{186}Pb and the distance between these levels may not be changed by more than a few hundreds of keV.

The prolate minimum is not as nicely related to a deformed proton shell effect, as no large gap is obtained for a deformation around β_2 equal to 0.3. The relation of this prolate configuration to a $4p$-$4h$ shell-model configuration is therefore not evident. In contrast, there is a small gap at the Fermi surface for β_2 values around 0.35, which corresponds to a $6p$-$6h$ configuration. A similar result has been obtained with the potential models used for microscopic-macroscopic calculations of Ref. [12].

As can be seen from Fig. 5, there are sizable neutron gaps at prolate deformations, which can be associated with structures in the potential energy curves, in particular, at $N=102$, $N=104$, and $N=106$ for $\beta_2 \approx 0.4$. These can be expected to enhance the depth of the prolate minimum in the potential landscape. Above $N=106$, the Fermi energy crosses a region of high level density, which explains the disappearance of the prolate minimum at neutron numbers above ^{190}Pb. The $N=102$ and $N=110$ gaps at larger deformations can be associated with the superdeformed minima in ^{184}Pb and ^{192}Pb, respectively.

C. Excitation spectra

The excitation spectra of $^{182-194}$Pb obtained after configuration mixing are presented in Fig. 6. The bars representing each state are plotted at a mean deformation $\overline{\beta}_{J,k}$ in the intrinsic frame defined as

$$\overline{\beta}_{J,k} = \int d\beta_2 \beta_2 \, g_{J,k}^2(\beta_2), \tag{8}$$

where β_2 is related to the value of the constraint used to generate the mean-field states [see Eq. (5)]. This average value does not correspond to any observable, but is convenient to characterize the decomposition of each collective state into its mean-field components. The collective wave functions for selected states are shown in Fig. 7. The fully correlated ground state is dominated by mean-field configurations close to sphericity for all isotopes, in agreement with the data. In $^{190-194}$Pb, the first excited 0^+ levels are dominated by oblate mean-field configurations. In ^{188}Pb, a configuration dominated by prolate mean-field states is nearly degenerate with the oblate one; for lighter isotopes, it becomes the first excited state.

For several isotopes, a classification of most states into rotational bands emerges quite naturally from the value of the average deformation $\overline{\beta}_{J,k}$. The simplest case is ^{190}Pb, where rotational bands above the oblate, prolate, and superdeformed configurations are easily identified in Fig. 6. An exception are the two nearly degenerated 6^+ levels found at intermediate deformations between the prolate and superdeformed bands which are very close in energy and, thus, strongly mixed. There is also an isolated 2^+ state with $\overline{\beta}_{2,3}$ close to 0 at 2.3 MeV excitation energy. Such a state is present at a similar energy in all other Pb isotopes studied here. The situation in ^{186}Pb is nearly as simple, except for two additional bands with average deformations between those of the first prolate and the superdeformed states. In the two lighter isotopes, the mean weight of oblate states in the

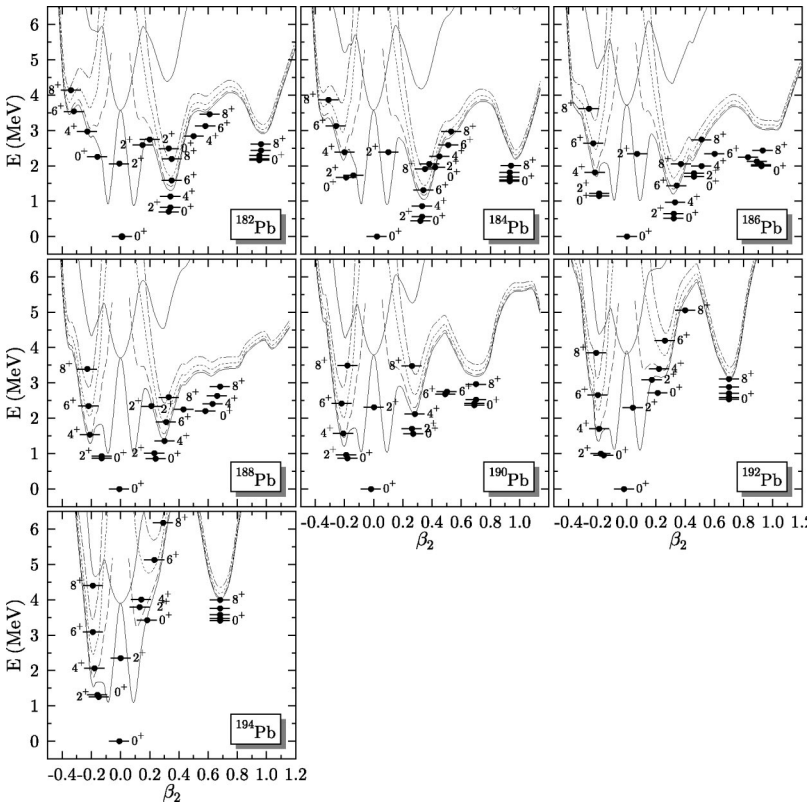

FIG. 6. Excited states in $^{182-194}$Pb. Only the lowest band structures are shown. For the superdformed bands, only the 0^+ and 8^+ levels are labeled.

predominantly oblate band is moving toward larger deformations with increasing spin, while the prolate band has a much more stable mean deformation. For ^{192}Pb and ^{194}Pb there are many levels above 4 MeV excitation energy that cannot be easily associated with a rotational band. Figure 7 indicates that the collective wave functions $g_{J,k}$ are spread over a large range of deformed configurations. For $J=0$ and 2, this spreading extends on both the prolate and oblate sides, while for $J=4$, it is more limited to the vicinity of either an oblate or a prolate configuration. Unfortunately, it is difficult to represent this spreading by the mixing of only two or three configurations, as done in schematic models. A reduction of the configuration mixing basis to an oblate, prolate, and spherical state leads to much too small a configuration mixing. Of course, the classification in bands that we have obtained from the $\overline{\beta}_{J,k}$ values has to be confirmed by the behavior of the calculated transition probabilities between the various states.

Our results concerning the lowest bands found in all isotopes are summarized in Fig. 8 (upper part) and compared to experimental data (lower part). Both for experiment and theory, the bands are sorted as oblate, prolate, or spherical on the basis of their spectroscopic properties.

Experimental trends are qualitatively reproduced by our calculation, although changes with neutron number are too abrupt. Our calculation predicts nearly degenerate oblate and prolate 0^+ excited states in ^{188}Pb only, while experimentally the two first excited 0^+ states lie within 100 keV in $^{184-188}$Pb. A systematic discrepancy between theory and experiment is the position of the 2^+ level interpreted as a vibration of the spherical ground state. Its energy is larger than 2 MeV in our calculation for all isotopes, a value to be compared with an experimental energy around 1 MeV [25]. Looking back into Fig. 7, a plausible reason for the better agreement obtained for the prolate states than for the other levels may lie in the behavior of the wave functions. For all isotopes, the ground state 0^+ wave functions have an extension on the oblate side similar to the predominantly oblate wave function. On the other hand, the amplitude of this wave function is negligible for deformations close to that of the maximum of the prolate wave function. Therefore, the configurations close to sphericity should be expected to be coupled more strongly to the oblate configurations than to the prolate ones. Such a strong coupling pushes the predominantly oblate 0^+ states higher in energy than the predominantly prolate ones. A similar explanation can be invoked to account for the too high energy of the vibrational 2^+ level constructed on the ground state. The wave function of this level extends on both prolate and oblate sides up to the tails of the oblate and prolate 2^+ wave functions. A possible way to reduce these large overlapping regions of collective wave functions could be the inclusion of triaxial deformation, which might lead to a different spreading of wave functions in the γ direction. There is also another possible explanation for the too large excitation energy of the calculated spherical 2^+ level for all nuclei. Since our wave functions are time-reversal invariant, they do not include two-quasiparticle excitations with nonzero spin. For small deformations, these states might be at lower excitation energy than the 2^+ states projected out from the BCS states that are included in our calculation. Therefore, introducing such two-quasiparticle states into the variational space for the GCM might affect mainly the spherical 2^+ states and decrease their excitation energy.

Experimental prolate states are nicely described by our calculations, although the increase of their excitation ener-

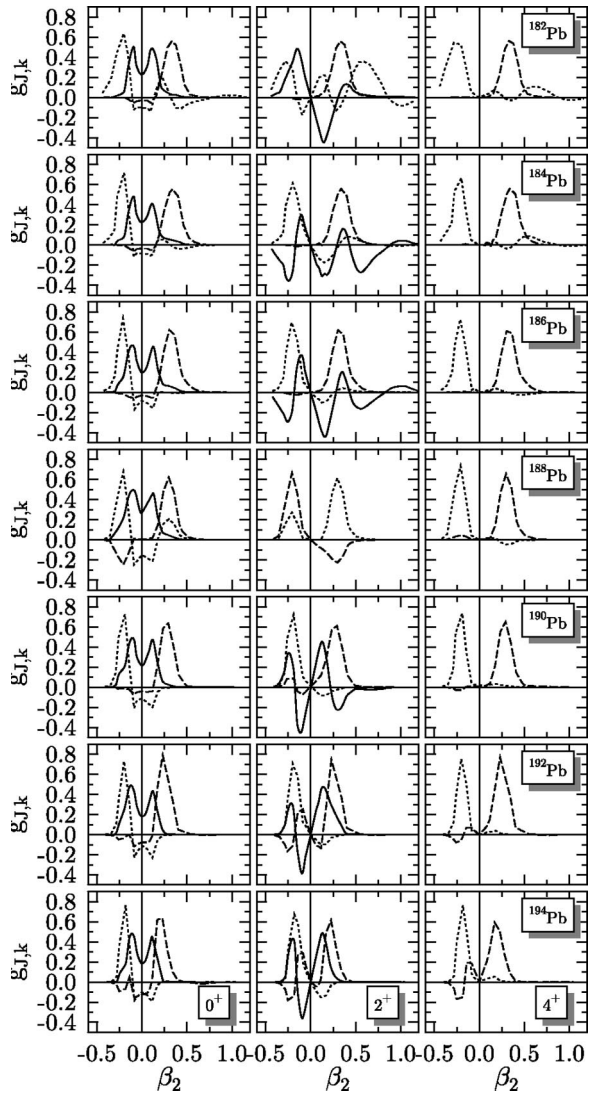

FIG. 7. Collective wave functions $g_{J,k}$, i.e., the amplitude of the deformed mean-field states in the collective states, of the three first 0^+ states at normal deformation for $^{182-194}$Pb. The predominantly spherical states are drawn with solid lines, while the predominantly prolate (oblate) states are drawn with dashed (dotted) lines, respectively.

gies with mass is slightly too fast for the heaviest isotopes. The simple picture of shape isomerism, as suggested by the potential landscapes, is supported by our calculations for oblate states, even after the inclusion of dynamical correlations on top of the shallow minima. This result is by far nontrivial. However, the position of these states is slightly too high in energy and the trend with neutron number is not correct. In particular, the excitation energy of the oblate isomer is not minimal at mid shell as it is experimentally. The minimum is shifted by four mass units towards heavier systems. The same situation is encountered in calculations using the Gogny force [17].

There are very recent new experimental data for ^{188}Pb [25,41]. In particular, this isotope is the one for which there are the most extensive data on $E0$ and $E2$ transition probabilities. For this reason, we show a direct comparison between theoretical and experimental spectra for this nucleus in Fig. 9. The main discrepancies with the data are for spins larger than four where the theoretical spectra are too spread. Experimentally, there is no clear evidence that the two first excited 0^+ levels are predominantly prolate or oblate in character. Starting at $J=2$, the states may be sorted in two bands fitted by a Harris expansion. This is also the case in our calculation. Experimentally, the lowest 2^+ state is interpreted as a member of the prolate band, while it belongs to the oblate one in our calculation.

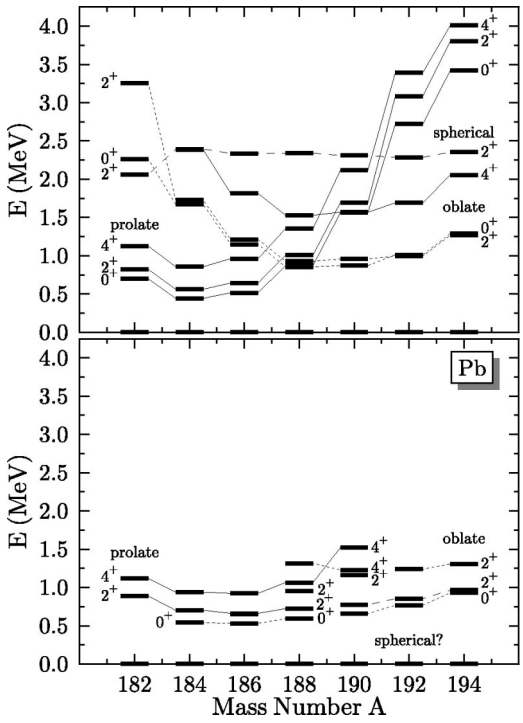

FIG. 8. Systematics of calculated (upper panel) and experimental (lower panel) excited states in $^{182-194}$Pb.

D. Correlation energies

From Fig. 6, one can extract the correlation energies due to the restoration of the rotational symmetry and the removal

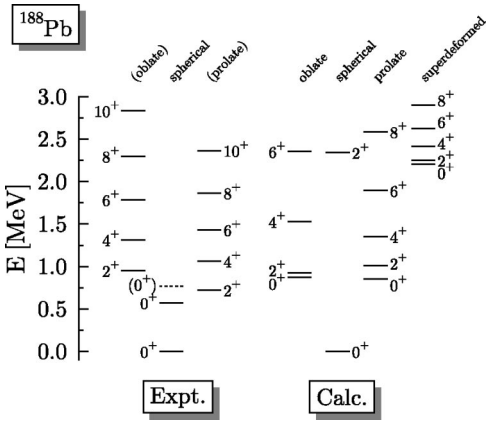

FIG. 9. Comparison between the calculated excitation energies and the available experimental data for low-lying states in ^{188}Pb. Data are taken from Ref. [25].

of axial quadrupole vibrations. Projection on particle number is already included in the mean-field energy curves. The magnitude of the correlation energy due to this projection has been determined in a previous study of Pb isotopes [42], and is around 1.0 MeV. The ground states are found to be spherical, irrespective of the nature of the correlations that are introduced. The rotational energy has a value close to 2.5 MeV in all cases and vibrational correlations bring an additional energy gain of approximately 1.0 MeV. The total energy gain due to these two correlations is rather stable for $^{182-194}$Pb and is comprised between 3.5 and 4.5 MeV.

E. Quadrupole deformation

1. Spectroscopic quadrupole moment

The spectroscopic quadrupole moment is given by

$$Q_c(J_k) = \sqrt{\frac{16\pi}{5}}\langle J,M=J,k|\hat{Q}_{20}|J,M=J,k\rangle$$
$$= \sqrt{\frac{16\pi}{5}}\frac{\langle JJ20|JJ\rangle}{\sqrt{2J+1}} \times \sum_{q,q'} f^*_{J,k}(q) f_{J,k}(q')\langle Jq||\hat{Q}_{20}||Jq'\rangle, \tag{9}$$

where $\hat{Q}_{20}$ is the proton quadrupole operator. Although directly accessible in a model-independent way in the laboratory frame, the spectroscopic quadrupole moment has the disadvantage that its value scales with mass and angular momentum. It is then difficult to compare different nuclei or different members of the same rotational band. Using the static rotor model, one can define a dimensionless quadrupole deformation in the intrinsic frame $\beta_2^{(s)}(J_k)$ which is easier to visualize and to relate to the deformation parameters introduced in most other models:

$$\beta_2^{(s)}(J_k) = \sqrt{\frac{5}{16\pi}}\frac{4\pi Q_2^{(s)}(J_k)}{3R^2Z},$$

$$Q_2^{(s)}(J_k) = -\frac{2J+3}{J}Q_c(J_k) \tag{10}$$

with $R=1.2A^{1/3}$ and $K=0$.

The absolute value of the deformation parameter $\beta_2^{(s)}$ derived from the spectroscopic quadrupole moment of low-lying 2^+ states is shown in Fig. 10. The β_2^s values corresponding to higher-lying members of the prolate and oblate rotational bands are in most cases quite similar to those obtained for the 2^+ state. In agreement with the systematics of the deformed minima in the potential energy surfaces shown in Figs. 1 and 3, the deformation of the prolate 2^+ levels increases with decreasing neutron number, while the deformation of the oblate 2^+ state stays fairly constant. The small values of $|\beta_2^{(s)}|$ found for the oblate 2^+ states in $^{182-184}$Pb and the prolate 2^+ states in $^{192-194}$Pb can be related to an increased spreading of the corresponding wave function into the spherical well due to the very small or even vanishing potential barrier in these cases. The discontinuity in the systematics of $\beta_2^{(s)}$ for oblate and prolate states predicted for ^{188}Pb is probably related to the increased mixing of all low-lying states due to their near degeneracy.

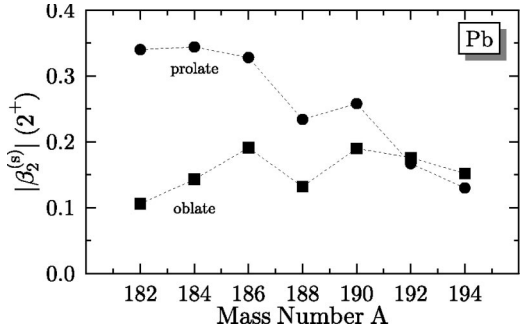

FIG. 10. Systematics of the intrinsic deformation $\beta_2^{(s)}$ derived from the absolute value of the spectroscopic quadrupole moment of low-lying 2^+ states in $^{182-194}$Pb. Circles denote prolate, squares oblate levels.

2. Reduced transition probabilities

The reduced $E2$ transition probability is determined from

$$B(E2;J'_{k'}\rightarrow J_k)$$
$$= \frac{e^2}{2J'+1}\sum_{M=-J}^{+J}\sum_{M'=-J'}^{+J'}\sum_{\mu=-2}^{+2}|\langle JMk|\hat{Q}_{2\mu}|J'M'k'\rangle|^2$$
$$= \frac{e^2}{2J'+1}\left|\sum_{q,q'} f^*_{J,k}(q) f_{J',k'}(q')\langle Jq||\hat{Q}_2||J'q'\rangle\right|^2. \tag{11}$$

The $B(E2)$ values are often given in Weisskopf units (W.u.), where 1 W.u. is equal to $5.940\times10^{-2}A^{4/3}e^2$ fm^4. Again, the $B(E2)$ value has the advantage that it can be deduced in a model-independent way in the laboratory frame, but also has the disadvantage that it scales with mass and angular momentum. Using the static rotor model, the $B(E2)$ values are related to a dimensionless deformation in the intrinsic frame

$$\beta_2^{(t)}(J'_{k'}\rightarrow J_k) = \frac{4\pi}{3R^2Z}\sqrt{\frac{B(E2;J'_{k'}\rightarrow J_k)}{\langle J'\ 0\ 2\ 0|J\ 0\rangle^2 e^2}} \tag{12}$$

with $R=1.2A^{1/3}$. This transition quadrupole moment reflects the intrinsic deformation of the states if, and only if, both states involved have a similar structure. Differences between $\beta_2^{(t)}(J'_{k'}\rightarrow J_k)$ and $\beta_2^{(s)}(J'_{k'})$ give a measure of the validity of the static rotor model for a given band.

The $\beta_2^{(t)}$ values derived from the transition probabilities between low-lying 4^+, 2^+, and 0^+ states are presented in Fig. 11. The values calculated for in-band transitions for higher J values are close to those for the $4^+\rightarrow2^+$ ones. Except for ^{184}Pb, very similar $\beta_2^{(t)}$ values are obtained for all transitions within the oblate band. On the contrary, the deformation determined from the $2^+_{\rm pro}\rightarrow0^+_{\rm pro}$ transition is significantly smaller than that calculated using the transition starting from the prolate 4^+ state. This is due to a change of structure of the collective wave functions with spin: the 0^+ wave functions are much more mixed than the wave functions corresponding to higher J values. The particularly large $\beta_2^{(t)}$ value found for

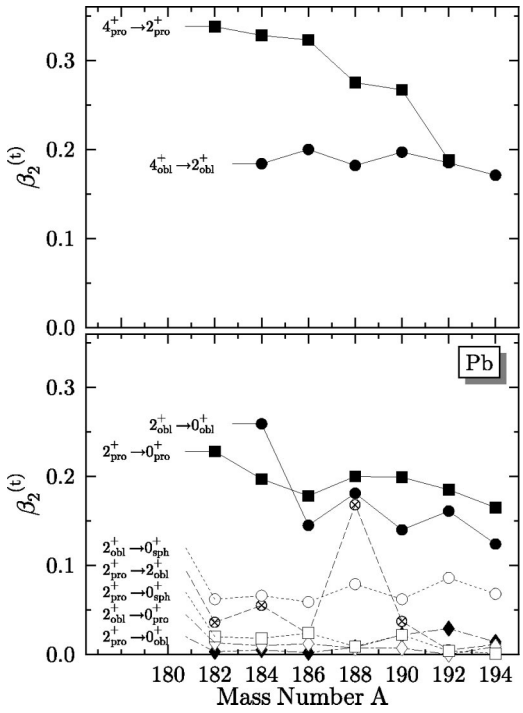

FIG. 11. Systematics of the intrinsic deformation derived from the reduced $E2$ transition probability between low-lying 2^+ and 0^+ states (lower panel) and low-lying 4^+ and 2^+ states (upper panel) in $^{182-194}$Pb. For in-band transitions between higher-lying states, $\beta_2^{(t)}$ values are similar to those obtained for the $4^+ \rightarrow 2^+$ transitions.

the $2^+_{pro} \rightarrow 2^+_{obl}$ transition in ^{188}Pb again reflects the large mixing of these two nearly degenerate states. From the right part of the figure, one sees that the in-band transitions are in most cases approximately one order of magnitude more intense than the out-of-band ones. Comparing the deformations calculated from the spectroscopic moments and shown in Fig. 10 to those coming from the transition moments, Fig. 11, one sees a close similarity, except for the oblate states in the two lightest isotopes and in ^{188}Pb. In these three cases, this can be viewed as a confirmation that the states labeled oblate result in fact from the mixing of a large range of mean-field states and that these mixings vary with angular momentum. The existence of rather pure rotational bands is confirmed for nuclei where both $\beta_2^{(t)}$ and $\beta_2^{(s)}$ have close values.

To the best of our knowledge, there are no experimental data for $B(E2)$ values in neutron-deficient Pb isotopes, except the very recent measurements in ^{188}Pb of Dewald *et al.* [41]. The $B(E2)$ value measured for the $4_1^+ \rightarrow 2_1^+$ transition is equal to 160 W.u. and that for the $2_1^+ \rightarrow gs$ transition is 5.3 W.u. These values are in between those that we obtain for transitions starting from the prolate and oblate 4^+ and 2^+ states. The calculated $B(E2)$ values for the $4_1^+ \rightarrow 2_1^+$ transition is equal to 288 W.u. for the prolate band and 126 W.u. for the oblate one, while the out-of-band transitions to the ground state are 0.2 W.u. and 17.0 W.u., respectively. This result probably reflects the fact that the calculation underestimates the configuration mixing for the 2^+ or the 4^+ states. Dewald *et al.* have determined a β_2 value of 0.20, significantly lower than the value obtained by most theoretical estimates. However, β_2 is not an observable and its value depends on the model used to relate it to the transition moments. The formula used in Ref. [41] contains a term coming from hexadecapole deformations which is usually not introduced. The determination of β_2 from the experimental data and Eq. (5) leads to a value compatible with the commonly estimated $\beta_2 = 0.27$.

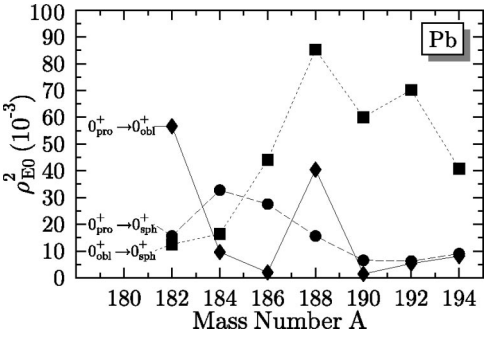

FIG. 12. Monopole strength ρ^2_{E0} for the transitions between low-lying 0^+ states. Available experimental data for the $0_2^+ \rightarrow 0_1^+$ transition in $^{190-194}$Pb are largely overestimated (see text).

F. Monopole transition moments

The $E0$ transition strength can be deduced from conversion-electron measurements. The formulas which relate decay rates and monopole strengths are a direct transposition to our model of the formulas given in Ref. [43].

The nuclear electric monopole decay rate $T(E0)$ due to conversion electrons is given by [44]

$$T(E0) = 2.786 \times 10^{20} \rho^2_{E0} \frac{\Delta E}{2J+1} \times [A(E0)_K + A(E0)_{L_I} + A(E0)_{L_{II}} + \cdots], \quad (13)$$

where $T(E0)$ is in s^{-1} and the transition energy ΔE in MeV. The electronic coefficients $A(E0)_i$, where i represents the decay channel, i.e., one of the electronic shells K, L_I, L_{II},…, have been tabulated by Hager and Selzer [45].

The nuclear matrix element entering this decay rate is the strength

$$\rho^2_{E0}(J_{k'} \rightarrow J_k) = \left| \frac{M(E0; J_{k'} \rightarrow J_k)}{R^2} \right|^2, \quad (14)$$

where $M(E0; J_{k'} \rightarrow J_k) = \langle JMk | r_p^2 | JMk' \rangle$ and R is 1.2 $A^{1/3}$ fm.

The values calculated for the transitions between prolate, oblate, and spherical 0^+ states are shown in Figs. 12–14. Their systematics reflects the change of the potential landscapes that can be seen in Fig. 3. In most cases, the larger the energy difference between the spherical and the deformed minima, the smaller the value of ρ^2_{E0}. The ρ^2_{E0} values are quite small for transitions between prolate and oblate states, except for ^{188}Pb where the two states are very close in energy and the oblate and prolate configurations are strongly mixed.

Experimental values for the monopole strength for the $(0_2^+ \rightarrow 0^+)$ transitions in $^{190-194}$Pb are given in Ref. [46]: $\rho^2_{E0} \geqslant 6 \times 10^{-3}$ for ^{190}Pb, $\rho^2_{E0} = (1.7 \pm 0.2) \times 10^{-3}$ for ^{192}Pb, and $\rho^2_{E0} = (1.0 \pm 0.2) \times 10^{-3}$ for ^{194}Pb. Assuming that the observed

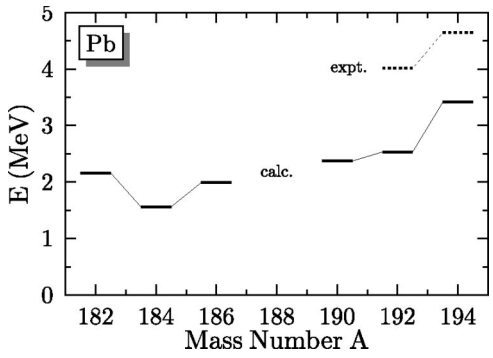

FIG. 13. Excitation energy of the 0^+ bandheads of the superdeformed rotational bands in $^{182-194}$Pb.

0_2^+ states can be identified with our oblate 0^+ levels, our calculations overestimate these values by more than one order of magnitude for ^{192}Pb and ^{194}Pb. Interestingly, transitions from the prolate 0^+ states to the ground state have the correct order magnitude.

If one estimates the mixing of configurations by the phenomenological formula used in Ref. [46],

$$\rho_{E0}^2 = a^2 b^2 \left(\frac{3Z}{4\pi}\right)^2 \beta^4, \tag{15}$$

where a and b (with $a^2 = 1 - b^2$) are the amplitudes of the spherical and oblate states in the physical wave functions, one obtains a mixing of around 10% in our calculation, 20 to 30 times larger than the value deduced from the experimental data. Even though Eq. (15) gives an extremely simple and approximate picture of the configuration, it confirms that our calculation probably predicts a much too large mixing between the spherical and oblate configurations.

Ratios of $E0$ and $E2$ transition probabilities for ^{188}Pb have been experimentally determined by Dracoulis *et al.* [25]. These data are for transitions between states of the oblate and prolate bands with the same angular momentum. For $J=2$, they obtain a ratio equal to 2.6, to be compared with 9.2 in our calculation, 2.2 for $J=4$, 1.2 for $J=6$, and 0.3 for $J=8$, to be compared with our calculated values of 0.27, 0.005, and 0.002, respectively.

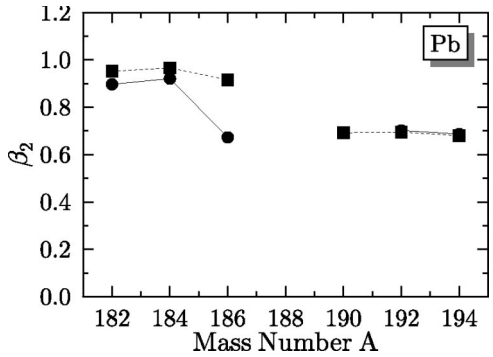

FIG. 14. Deformation of the SD states. Squares, $\beta_2^{(s)}$ of the 2^+ states; circles, $\beta_2^{(t)}(6^+ \rightarrow 4^+)$ (for $^{190-194}$Pb, they lie on top of each other).

Using a simple band-mixing model adjusted using the experimental data, Dracoulis *et al.* [25] have determined the widths of all the $E0$ and $E2$ transitions depopulating the oblate band. Our model also allows to determine these widths, without any additional assumptions. The widths of the dominant $E2$ transitions differ by at most an order of magnitude; differences are larger for $E0$ transitions, where our calculated values are lower by a factor varying from 10 for $J=2$ to 500 for $J=6$. In the model of Dracoulis *et al.*, all states result from the mixing of a prolate and an oblate configuration only, while the mixing is much more complicated in our calculation. The lower value for the $E0$ width that we obtain is probably related to larger differences in structure between the oblate and prolate bands in the present calculation than in schematic models. The quadrupole transitions are in better agreement with the data. The widths that can be calculated from the data of Dewald *et al.* [41] agree with our computed values within a factor 2.

IV. SUPERDEFORMED STRUCTURES

Superdeformed bands have been extensively studied utilizing the cranked HFB method (see Ref. [47] and references therein). In this approach, the variation of the moment of inertia of a rotational band is studied up to high spins by means of mean-field states optimized for each angular momentum with an appropriate cranking constraint. The variational space of the CHFB method is larger than in the present calculations due to the breaking of time-reversal invariance. As long as rotation takes place in a potential well which does not vary too much with rotation, the cranking approximation is rather well justified. Because of this feature, it is also well suited to describe the moment of inertia of SD bands.

To challenge CHFB calculations, our method requires to project cranked HFB states on angular momentum; such a generalization is underway. Nevertheless, we have extended our calculations to deformations at which superdeformed rotational bands have been observed in $^{192-196}$Pb. Figure 6 shows the spectra obtained in the SD well after symmetry restorations and configuration mixing. Compared to experiment, and to our previous CHFB calculation [48], the SD spectra are too compressed and the moments of inertia too large. As the interaction that we used in Ref. [48] was the SLy4 Skyrme parametrization, we checked that the SLy6 parametrization used here leads to similar rotational bands when used in CHFB calculations and that agreement with the experimental data is equally good. Without cranking, our results for SD spectra cannot provide an accurate quantitative comparison with experiment. However, our present method is very well adapted to determine the excitation energy of the SD well. As a matter of fact, it can be viewed as a generalization of the method that we have already applied to the same problem [49] as correlations due to the restoration of angular momentum are included. Looking at Fig. 6, one sees that bands are very well localized in the superdeformed well for $^{190-194}$Pb. Quadrupole deformations are slightly larger than in our cranking studies, with typical values of β_2 around 0.70, compared to 0.67 in CHFB for SLy4 and SLy6.

Transitions linking the SD bands to the normal-deformed well are known in ^{194}Pb [50,51] and, recently, in ^{192}Pb [52].

From these transitions one can estimate the "experimental" position of the 0^+ bandheads in these two nuclei. Calculated excitation energies of 2.5 MeV for ^{192}Pb and 3.4 MeV for ^{194}Pb, are below the extrapolated experimental values of 4.425 MeV for ^{192}Pb and 4.878 MeV for ^{194}Pb. We have repeated the same calculation with the SLy4 interaction used in a systematic study of the excitation energies of SD bands [53,54] and obtained 4.7 MeV for ^{194}Pb. This value is in much better agreement with the data. This difference between both interactions gives a measure of the uncertainty related to the choice of the effective interaction.

A detailed analysis shows that the excitation energy of the SD band is substantially modified by the correlations. For ^{194}Pb for instance, the excitation energy of the superdeformed minimum in the potential energy surface is lowered by angular momentum projection from 3.9 MeV to 3.0 MeV, see Figs. 1 and 3. But after configuration mixing, the superdeformed 0^+ state is pushed up again to 3.41 MeV. As can be seen in Fig. 6, quadrupole vibrations lower the SD state even further than the projection, but this effect is larger for the ground state, so the SD bandheads are actually pushed toward larger excitation energy. For ^{192}Pb, angular momentum projection reduces the excitation energy from 3.0 MeV to 2.0 MeV, while the quadrupole correlations increase it back to 2.53 MeV. In the same way, using the SLy4 interaction, the excitation energy of the SD band in ^{194}Pb is first reduced from 5.2 MeV to 4.3 MeV and then increased back to 4.71 MeV by the GCM. A similar reduction of the excitation energy of SD bandheads in spherical nuclei was obtained for ^{16}O [28] and ^{40}Ca [33]. In those light nuclei, the absolute change of the excitation energy is more pronounced.

No stable states are obtained in the SD well of ^{188}Pb. For lighter isotopes, well-defined states are obtained again at large deformation. They form nice rotational bands for ^{184}Pb and ^{182}Pb. Their excitation energies are quite small, below 3 MeV, see Fig. 6, even if one takes the uncertainty due to the interaction into account. Their quadrupole moment is also significantly larger than for the known SD bands, leading to very strong $B(E2)$ transition probabilities within the bands.

V. DISCUSSION AND SUMMARY

The main aim of this paper was to determine whether it is possible to describe the coexistence of several low-lying 0^+ states in neutron-deficient Pb isotopes by introducing correlations. In this respect, our results are very positive. The evolution of the Pb spectra with neutron number is qualitatively well reproduced. The direct link between symmetry restored wave functions and intrinsic mean-field configurations allows to assign a predominantly oblate structure to the first excited 0^+ state in the heaviest Pb isotopes and a predominantly prolate one in the lightest ones. This result was not evident from *a priori* analyses of the mean-field deformation energy curves. In several cases, the deformed minima are located in a well not expected to be sufficiently deep to guarantee the localization of a quantum state. Our results, obtained from a purely quantum mechanical method based on an effective interaction as the sole phenomenological ingredient, do support the intuitive shape coexistence picture.

More detailed comparisons with the data show some discrepancies. While the energies of the predominantly prolate states reproduce the experimental data qualitatively, the energies of the oblate ones are systematically overestimated and the spreading of the rotational bands is too large. There could be different origins for these discrepancies. First, the lack of triaxial deformations could induce an overestimation of the energy of the oblate configuration. Their introduction should increase the coupling between prolate and oblate states which seems to be too weak when looking into $E0$ transition probabilities in ^{188}Pb. Second, mean-field states are generated by static calculations. This is not satisfactory from a variational point of view. As is well known, the projection of cranked states obtained for $J_x = J$ is better variationally and is expected to decrease the spreading of the bands. Such an extension of our method is by far not trivial, but is presently underway.

Finally, the effective interactions have not been constructed to go beyond a mean-field approach. In principle, they should be readjusted, at least to account for the extra binding energies due to rotational and vibrational correlations. Furthermore, our results could be affected by considering other generalizations of the density dependence of the Skyrme force when calculating nondiagonal matrix elements, as suggested by Duguet and Bonche [55,56]. Such an investigation is presently underway. Even at the mean-field level, deficiencies of the Skyrme interactions have been put into evidence. The analysis of the single-particle spectra in ^{208}Pb and ^{249}Bk matches up with the conclusion drawn here from the neutron-number dependence of the oblate configuration that the proton $1i_{13/2^+}$ shell is calculated too high in excitation energy, above the $1h_{9/2^-}$ level. This is a feature common to many effective interactions which should be taken into account in a new fit of a force.

One of the major interests of our method is the determination of transition probabilities directly in the laboratory system, without relying on ad hoc approximations. Unfortunately, the experimental data are very limited. The example of ^{188}Pb has shown how instructive the comparison between theory and experiment for $E0$ and $E2$ transition probabilities can be. Experimental data for other isotopes are highly desirable.

Finally, we have extended our calculations up to quadrupole deformations associated with superdeformed bands. As expected, for the isotopes in which these bands are known, the excitation energies are in reasonable agreement with experiment, but the moments of inertia are too large and not as good as in our previous cranking calculations. While the disappearance of SD structures is confirmed in $^{188-190}$Pb, still more deformed configurations are predicted in the lightest isotopes. The experimental confirmation of this prediction is certainly a difficult experimental challenge, but would be an exciting result.

ACKNOWLEDGMENTS

This research was supported in part by the PAI-P5-07 of the Belgian Office for Scientific Policy, and by the U.S. De-

partment of Energy (DOE), Nuclear Physics Division, under Contract No. W-31-109-ENG-38. M.B. acknowledges financial support by the European Community. We thank G. Dracoulis, K. Heyde, M. Huyse, R. V. F. Janssens, R. Julin, G. Neyens, and P. Van Duppen for fruitful discussions. We acknowledge the hospitality of ECT*, the European Centre for Theoretical Studies in Nuclear Physics and Related Areas, Trento, where this work was finalized.

[1] R. Julin, K. Helariutta, and M. Muikki, J. Phys. G **27**, R109 (2001).
[2] P. Van Duppen, E. Coenen, K. Deneffe, M. Huyse, K. Heyde, and P. Van Isacker, Phys. Rev. Lett. **52**, 1974 (1984).
[3] P. Van Duppen, E. Coenen, K. Deneffe, M. Huyse, and J. L. Wood, Phys. Rev. C **35**, 1861 (1987).
[4] A. N. Andreyev, M. Huyse, P. Van Duppen, L. Weissman, D. Ackermann, J. Gerl, F. Heßberger, S. Hofmann, A. Kleinbohl, G. Münzenberg, S. Reshitko, C. Schlegel, H. Schaffner, P. Cagarda, M. Matos, S. Saro, A. Keenan, C. J. Moore, C. D. O'Leary, R. D. Page, M. J. Taylor, H. Kettunen, M. Leino, A. Lavrentiev, R. Wyss, and K. Heyde, Nature (London) **405**, 430 (2000); Nucl. Phys. **A682**, 482c (2001).
[5] J. Heese, K. H. Maier, H. Grawe, J. Grebosz, H. Kluge, W. Meczynski, M. Schramm, R. Schubart, K. Spohr, and J. Styczen, Phys. Lett. B **302**, 390 (1993).
[6] A. M. Baxter, A. P. Byrne, G. D. Dracoulis, R. V. F. Janssens, I. G. Bearden, R. G. Henry, D. Nisius, C. N. Davids, T. L. Khoo, T. Lauritsen, H. Penttilä, D. J. Henderson, and M. P. Carpenter, Phys. Rev. C **48**, R2140 (1993).
[7] W. Reviol, C. J. Chiara, O. Pechenaya, D. G. Sarantites, P. Fallon, and A. O. Macchiavelli, Phys. Rev. C **68**, 054317 (2003).
[8] J. Wauters, N. Bijnens, H. Folger, M. Huyse, Han Yull Hwang, R. Kirchner, J. von Schwarzenberg, and P. Van Duppen, Phys. Rev. C **50**, 2768 (1994).
[9] J. L. Wood, K. Heyde, W. Nazarewicz, M. Huyse, and P. Van Duppen, Phys. Rep. **215**, 101 (1992).
[10] K. Heyde, P. Van Isacker, M. Waroquier, J. L. Wood, and R. A. Meyer, Phys. Rep. **102**, 291 (1983).
[11] F. R. May, V. V. Pashkevich, and S. Frauendorf, Phys. Lett. **68B**, 113 (1977).
[12] R. Bengtsson and W. Nazarewicz, Z. Phys. A **334**, 269 (1989).
[13] W. Satuła, S. Ćwiok, W. Nazarewicz, R. Wyss, and A. Johnson, Nucl. Phys. **A529**, 289 (1991).
[14] W. Nazarewicz, Phys. Lett. B **305**, 195 (1993).
[15] N. Tajima, H. Flocard, P. Bonche, J. Dobaczewski, and P.-H. Heenen, Nucl. Phys. **A551** 409 (1993).
[16] J. Libert, M. Girod, and J.-P. Delaroche, Phys. Rev. C **60**, 054301 (1999).
[17] R. R. Chasman, J. L. Egido, and L. M. Robledo, Phys. Lett. B **513**, 325 (2001).
[18] T. Nikšić, D. Vretenar, P. Ring, and G. A. Lalazissis, Phys. Rev. C **65**, 054320 (2002).
[19] K. Heyde, J. Schietse, and C. De Coster, Phys. Rev. C **44**, 2216 (1991).
[20] C. De Coster, B. Decroix, and K. Heyde, Phys. Rev. C **61**, 067306 (2000).
[21] R. Fossion, K. Heyde, G. Thiamova, and P. Van Isacker, Phys. Rev. C **67**, 024306 (2003).
[22] P. Van Duppen, M. Huyse, and J. L. Wood, J. Phys. G **16**, 441 (1990).
[23] D. S. Delion, A. Florescu, M. Huyse, J. Wauters, P. Van Duppen, A. Insolia, and R. J. Liotta, Phys. Rev. C **54**, 1169 (1996).
[24] R. G. Allatt, R. D. Page, M. Leino, T. Enqvist, K. Eskola, P. T. Greenlees, P. Jones, R. Julin, P. Kuusiniemi, W. H. Trzaska, and J. Uusitalo, Phys. Lett. B **437**, 29 (1998).
[25] G. D. Dracoulis, G. J. Lane, A. P. Byrne, A. M. Baxter, T. Kibédi, A. O. Macchiavelli, P. Fallon, and R. M. Clark, Phys. Rev. C **67**, 051301(R) (2003).
[26] K. Heyde and R. A. Meyer, Phys. Rev. C **37**, 2170 (1988).
[27] A. Valor, P.-H. Heenen, and P. Bonche, Nucl. Phys. **A671**, 145 (2000).
[28] M. Bender and P.-H. Heenen, Nucl. Phys. **A713**, 390 (2003).
[29] T. Duguet, M. Bender, P. Bonche, andP.-H. Heenen, Phys. Lett. B **559**, 201 (2003).
[30] D. L. Hill and J. A. Wheeler, Phys. Rev. **89**, 1102 (1953); J. J. Griffin and J. A. Wheeler, *ibid.* **108**, 311 (1957).
[31] E. Chabanat, P. Bonche, P. Haensel, J. Meyer, and R. Schaeffer, Nucl. Phys. **A635**, 231 (1998); **A643**, 441(E) (1998).
[32] C. Rigollet, P. Bonche, H. Flocard, and P.-H. Heenen, Phys. Rev. C **59**, 3120 (1999).
[33] M. Bender, H. Flocard, and P.-H. Heenen, Phys. Rev. C **68**, 044321 (2003).
[34] S. Ćwiok (private communication).
[35] G. J. Lane, G. D. Dracoulis, A. P. Byrne, P. M. Walker, A. M. Baxter, J. A. Sheikh, and W. Nazarewicz, Nucl. Phys. **A586**, 316 (1995).
[36] K. Vyvey, A. M. Oros-Peusquens, G. Neyens, D. L. Balabanski, D. Borremans, S. Chmel, N. Coulier, R. Coussement, G. Georgiev, H. Hübel, N. Nenoff, D. Rossbach, S. Teughels, and K. Heyde, Phys. Lett. B **538**, 33 (2002); K. Vyvey, D. Borremans, N. Coulier, R. Coussement, G. Georgiev, S. Teughels, G. Neyens, H. Hübel, and D. L. Balabanski, Phys. Rev. C **65**, 024320 (2002); K. Vyvey, S. Chmel, G. Neyens, H. Hübel, D. L. Balabanski, D. Borremans, N. Coulier, R. Coussement, G. Georgiev, N. Nenoff, S. Pancholi, D. Rossbach, R. Schwengner, S. Teughels, and S. Frauendorf, Phys. Rev. Lett. **88**, 102502 (2002).
[37] N. A. Smirnova, P.-H. Heenen, and G. Neyens, Phys. Lett. B **569**, 151 (2003).
[38] M. Bender, P. Bonche, T. Duguet, and P.-H. Heenen, Nucl. Phys. **A723**, 354 (2003).
[39] M. Bender, K. Rutz, P.-G. Reinhard, J. A. Maruhn, and W. Greiner, Phys. Rev. C **60**, 034304 (1999).
[40] M. Kleban, B. Nerlo-Pomorska, J. F. Berger, J. Dechargé, M. Girod, and S. Hilaire, Phys. Rev. C **65**, 024309 (2002).
[41] A. Dewald, R. Peusquens, B. Saha, P. von Brentano, A. Fitzler, T. Klug, I. Wiedenhöver, M. P. Carpenter, A. Heinz, R. V. F. Janssens, F. G. Kondev, C. J. Lister, D. Seweryniak, K. Abu Saleem, R. Krücken, J. R. Cooper, C. J. Barton, K. Zyromski, C. W. Beausang, Z. Wang, P. Petkov, A. M. Oros-Peusquens,

U. Garg, and S. Zhu, Phys. Rev. C **68**, 034314 (2003).
[42] P.-H. Heenen, A. Valor, M. Bender, P. Bonche, and H. Flocard, Eur. Phys. J. A **11**, 393 (2001).
[43] H. Dancer, P. Bonche, H. Flocard, P.-H. Heenen, J. Meyer, and M. Meyer, Phys. Rev. C **58**, 2068 (1998).
[44] E. L. Church and J. Weneser, Phys. Rev. **103**, 1035 (1956).
[45] R. S. Hager and E. C. Seltzer, Nucl. Data, Sect. A **6**, 1 (1969).
[46] P. Dendooven, P. Decrock, M. Huyse, G. Reusen, P. Van Duppen, and J. Wauters, Phys. Lett. B **226**, 27 (1989).
[47] M. Bender, P.-H. Heenen, and P.-G. Reinhard, Rev. Mod. Phys. **75**, 121 (2003).
[48] J. Terasaki, P.-H. Heenen, P. Bonche, J. Dobaczewski, and H. Flocard, Nucl. Phys. **A593**, 1 (1995); P. Fallon, P.-H. Heenen, W. Satuła, R. M. Clark, F. S. Stephens, M. A. Deleplanque, R. M. Diamond, I. Y. Lee, A. O. Macchiavelli, and K. Vetter, Phys. Rev. C **60**, 044301 (1999).
[49] J. Meyer, P. Bonche, M. S. Weiss, J. Dobaczewski, H. Flocard, and P.-H. Heenen, Nucl. Phys. **A588**, 597 (1995).
[50] A. Lopez-Martens, F. Hannachi, A. Korichi, C. Schück, E. Gueorguieva, Ch. Vieu, B. Haas, R. Lucas, A. Astier, G. Baldsiefen, M. Carpenter, G. de France, R. Duffait, L. Ducroux, Y. Le Coz, Ch. Finck, A. Gorgen, H. Hübel, T. L. Khoo, T. Lauritsen, M. Meyer, D. Prévost, N. Redon, C. Rigollet, H. Savajols, J. F. Sharpey-Schafer, O. Stezowski, Ch. Theisen, U. Van Severen, J. P. Vivien, and A. N. Wilson, Phys. Lett. B **380**, 18 (1996).
[51] R. Krücken, S. J. Asztalos, J. A. Becker, B. Busse, R. M. Clark, M. A. Deleplanque, A. Dewald, R. M. Diamond, P. Fallon, K. Hauschild, I. Y. Lee, A. O. Macchiavelli, R. W. MacLeod, R. Peusquens, G. J. Schmid, F. S. Stephens, K. Vetter, and P. von Brentano, Phys. Rev. C **55**, R1625 (1997)
[52] A. N. Wilson, G. D. Dracoulis, A. P. Byrne, P. M. Davidson, G. J. Lane, R. M. Clark, P. Fallon, A. Görgen, A. O. Macchiavelli, and D. Ward, Phys. Rev. Lett. **90**, 142501 (2003).
[53] P.-H. Heenen, J. Dobaczewski, W. Nazarewicz, P. Bonche, and T. L. Khoo, Phys. Rev. C **57**, 1719 (1998).
[54] P. Bonche, J. Dobaczewski, H. Flocard, P.-H. Heenen, and J. Meyer, Nucl. Phys. **A510**, 466 (1990).
[55] T. Duguet, Phys. Rev. C **67**, 044311 (2003).
[56] T. Duguet and P. Bonche, Phys. Rev. C **67**, 054308 (2003).